

OPEN

Novel Unexpected Reconstructions of (100) and (111) Surfaces of NaCl: Theoretical Prediction

Alexander G. Kvashnin^{1,2}, Dmitry G. Kvashnin^{3,4} & Artem R. Oganov^{1,2,5}

We have predicted stable reconstructions of the (100) and (111) surfaces of NaCl using the global optimization algorithm USPEX. Several new reconstructions, together with the previously reported ones, are found. For the cleaved bare (100) surface, pure Na and pure Cl are the only stable surface phases. Our study of the (111) surface shows that a newly predicted $\text{Na}_3\text{Cl}-(1 \times 1)$ reconstruction is thermodynamically stable in a wide range of chlorine chemical potentials. It has a sawtooth-like profile where each facet reproduces the (100) surface of rock-salt NaCl, hinting on the preferred growth of the (100) surface. We used Bader charge analysis to explain the preferable formation of this sawtooth-like $\text{Na}_3\text{Cl}-(1 \times 1)$ reconstruction of the (111) surface of NaCl. We find that at a very high chemical potential of Na, the polar (and normally absent) (111) surface becomes part of the equilibrium crystal morphology. At both very high and very low chemical potentials of Cl, we predict a large decrease of surface energy and fracture toughness (the Rebinder effect).

One of the simplest and most thoroughly studied ionic crystals is sodium chloride, also known as table salt. It is well established that NaCl has a B1 (“rock-salt”) structure that transforms into the CsCl-type structure (the B2 phase) at about 30 GPa and room temperature¹. A number of theoretical² and experimental³ studies confirm that only these two phases exist in the 0–300 GPa pressure range. At a negative pressure, a wurtzite-type phase of NaCl was predicted⁴. Several stable Na_xCl_y phases of various unusual stoichiometries were discovered at pressures above 22 GPa in ref.⁵. Two of these exotic compounds, Na_3Cl and Na_2Cl , were found at normal conditions as stable 2D phases on a graphene substrate⁶.

In contrast to the bulk case, a completely different situation may occur at low dimensions, e.g. in thin films and on surfaces. The available reference data show that the most energetically favorable surface of NaCl is (100)^{7–9}. This was confirmed by a number of experimental and theoretical studies, where thin films of sodium chloride with the (100) surface orientation were grown on various substrates, namely Cu(001)^{10,11}, Cu(110)¹², Cu(111)^{13–19}, Cu(311)²⁰, Cu(221)^{20,21}, Ni(001)¹¹, Ag(001)^{19,22–24}, Ag(111)^{19,25,26}, Au(111) and Au(111)-(22 × $\sqrt{3}$)²⁷. In addition, it was shown by Kiguchi *et al.*¹¹ that the interaction between an alkali metal halide film and substrate is weak and the substrate does not influence the atomic structure of the grown films. Perhaps increasing the interaction between the substrate and film by selecting a particular substrate may lead to the formation of NaCl films with unusual structures.

Recent experiments on ultrathin films of various compounds show that thin films of zinc oxide (ZnO) terminated by a polar (0001) surface undergo a spontaneous splitting into graphene-like layers^{28,29}. Moreover, graphene-like thin films of silicon carbide (SiC) and aluminum nitride (AlN) were also synthesized^{30,31}. Detailed theoretical studies of the graphitization of thin films with different types of crystal structure, including NaCl with (111) surface, were reported^{32–34}. There are also several experimental studies of the growth of NaCl films corresponding to the (111) surface on various substrates. In ref.³⁵, the growth of NaCl(111) on the GaAs(111) surface was carried out using molecular beam epitaxy. As a result, an anomalous and unstable NaCl film with the (111) surface was obtained. Another appropriate substrate for growing alkali halides is silicon^{36,37}. Reconstructed surfaces of Si(100)-(2 × 1)³⁶ and Si(111)-(7 × 7)³⁷ were used as substrates for growing bilayer NaCl films with the

¹Skolkovo Institute of Science and Technology, Skolkovo Innovation Center, 3 Nobel Street, Moscow, 121205, Russia. ²Moscow Institute of Physics and Technology, 9 Institutsky Pereulok, Dolgoprudny, 141700, Russia. ³Emanuel Institute of Biochemical Physics RAS, 4 Kosigina Street, Moscow, 119334, Russia. ⁴National University of Science and Technology MISIS, 4 Leninskiy Prospekt, Moscow, 119049, Russia. ⁵International Center for Materials Discovery, Northwestern Polytechnical University, Xi’an, 710072, China. Correspondence and requests for materials should be addressed to D.G.K. (email: dgkvashnin@phystech.edu)

Received: 26 July 2019

Accepted: 12 September 2019

Published online: 03 October 2019

(100) surface³⁶ and thin islands of KCl with both the (111) and (100) surfaces³⁷. All the experimental evidence proves the energetic preference of the (100) surface of NaCl compared to the (111) surface, which, however, can also be obtained with sufficient care.

In all the above mentioned theoretical works the 2D films and surfaces were modeled assuming the fixed structure and composition equivalent to the bulk, without accounting for reconstructions and the effect of chemical potentials.

Here we search for thermodynamically stable reconstructions of the (100) and (111) surfaces of NaCl. We use the evolutionary algorithm USPEX^{38–41}, which makes it possible to determine stable reconstructions and predict the conditions of their formation. Several interesting reconstructions of the NaCl(111) surface were found and their stability conditions determined.

Results and Discussion

First we study the (100) surface of NaCl, for which we predicted several thermodynamically stable reconstructions shown in Fig. 1a. We name the predicted reconstructions using the stoichiometry difference between the whole structure and substrate. This nomenclature is standard and was used in a number of previous works^{42,43}. Four stable reconstructions were predicted, $\text{Cl}_6\text{-(}\sqrt{2} \times \sqrt{2}\text{)}$, $\text{Cl}_4\text{-(}1 \times 1\text{)}$, $\text{NaCl-(}1 \times 1\text{)}$, and $\text{Na}_2\text{-(}1 \times 1\text{)}$, of which only one has both sodium and chlorine in its surface composition, while the rest of them have either pure chlorine or pure sodium surfaces (Fig. 1a).

The stability of the predicted reconstructions and its dependence on the chemical potential of chlorine was investigated in more details by calculating the surface energy diagram (Fig. 1b). The widest stability region with μ_{Cl} between -1.86 eV and -3.69 eV belongs to the unreconstructed NaCl(100) surface, which is perfectly consistent with the experimental evidence^{13,14,44,45}. There are two reconstructions that can be formed under conditions of a chlorine excess, $\text{Cl}_6\text{-(}\sqrt{2} \times \sqrt{2}\text{)}$ and $\text{Cl}_4\text{-(}1 \times 1\text{)}$ (Fig. 1a). It is important that these chlorine-rich reconstructions are stable in very narrow ranges of chlorine chemical potentials (Fig. 1c) corresponding to the chlorine-rich environmental conditions. Another reconstruction, $\text{Na}_2\text{-(}1 \times 1\text{)}$, can be formed in a lack of chlorine (Fig. 1a), and can be described as a layer of NaCl adsorbed on the NaCl(100) surface. At very low chemical potentials of chlorine (i.e., very high chemical potentials of Na) and at very high chemical potentials of chlorine, the energy of the (100) surface is greatly diminished (Fig. 1b). We recall that surface energy is related to fracture toughness K_g ⁴⁶:

$$K_g = 2\sqrt{\gamma G/(1 - \nu)}, \quad (1)$$

where γ is the surface energy, G is the shear modulus, ν is the Poisson's ratio of the material.

Therefore, we expect that NaCl will become much more brittle when immersed in gaseous or liquid Na or Cl, the phenomenon known as the Rehbinder effect^{47–50}. Normally, the Rehbinder effect occurs because of a decrease in surface energy due to wetting; in our case it takes place because of the formation of new surface reconstructions that significantly reduce surface energy, which leads to a reduction in fracture toughness.

The calculated convex hull diagram is shown in Fig. 1d. A strong cusp corresponding to the nonreconstructed NaCl(100) surface indicates its stability in a wide range of chlorine chemical potentials, as seen in the surface diagram (Fig. 1b).

The calculated pressure-temperature phase diagram of the NaCl(100) surface shown in Fig. 1e makes it possible to predict the environmental conditions (partial chlorine pressure and temperature) suitable for the formation of a particular reconstruction. Both partial chlorine pressure and temperature are parts of the expression for chemical potential:

$$\mu_{\text{Cl}} = \frac{1}{2} \left[E_{\text{Cl}_2} + G_{\text{Cl}_2}(T, P_0) + k_B T \ln \left(\frac{P}{P_0} \right) \right] = \frac{1}{2} E_{\text{Cl}_2} + \Delta\mu_{\text{Cl}}(T, P), \quad (2)$$

where $G_{\text{Cl}_2}(T, P_0)$ is the calculated Gibbs free energy of the gas of chlorine molecules at a certain temperature and pressure, which agrees well with the data from the thermodynamic database⁵¹. The details of the calculations and comparison with the reference data are shown in Supporting Information Table S1.

The calculated phase diagram (Fig. 1e) shows stability of the $\text{Cl}_4\text{-(}1 \times 1\text{)}$ reconstruction at a chlorine partial pressure $>10^{-5}$ bar (dotted horizontal line in Fig. 1e) and temperatures <320 K. The phase boundary between the $\text{Cl}_4\text{-(}1 \times 1\text{)}$ and $\text{Cl}_6\text{-(}2 \times 1\text{)}$ reconstructions in Fig. 1e corresponds to $\mu_{\text{Cl}} = -1.84$ eV. Each phase boundary was plotted using Eq. (2) with the corresponding value of the chemical potential of chlorine. Increasing the temperature to 320 K at the chlorine partial pressure of 10^{-5} bar (dotted horizontal line) will lead to the formation of the $\text{Cl}_6\text{-(}2 \times 1\text{)}$ reconstruction with a very narrow stability region, shown in blue in Fig. 1e. Further increase in temperature to 400 K will lead to the formation of a cleaved bare NaCl(100) surface that has the largest stability field (orange region in Fig. 1e). The chlorine partial pressure of 4×10^{-9} bar (dashed horizontal line in Fig. 1e) corresponds to the experimental pressure conditions of the homoepitaxial NaCl growth, where the formation of the cleaved bare (100) surface was observed⁵². The temperatures of 300 K and 400 K from the experiment are shown by two white circles⁵². Our simulation is consistent with these experiments, where at chlorine pressures $<10^{-10}$ bar the cleaved bare NaCl(100) surface is stable in the whole temperature range up to the melting point of NaCl (~ 1100 K)⁵². Very low chlorine pressures $<10^{-20}$ bar lead to conditions of sodium excess with $\mu_{\text{Cl}} > -3.69$ eV. Such a low pressure, as well as high temperatures >900 K, lead to the formation of the $\text{Na}_2\text{-(}1 \times 1\text{)}$ reconstruction, shown in red in Fig. 1e.

The NaCl(111) surface is much more interesting. It is polar and has a higher surface energy γ compared to the (100) surface: the values of 0.024 eV/Å² (ref.⁵³) or 0.033 eV/Å² (ref.⁵⁴) were computed for the (111) surface vs. 0.01 eV/Å² computed for the (100) surface⁵³. Our calculations give similar values for the surface energies of

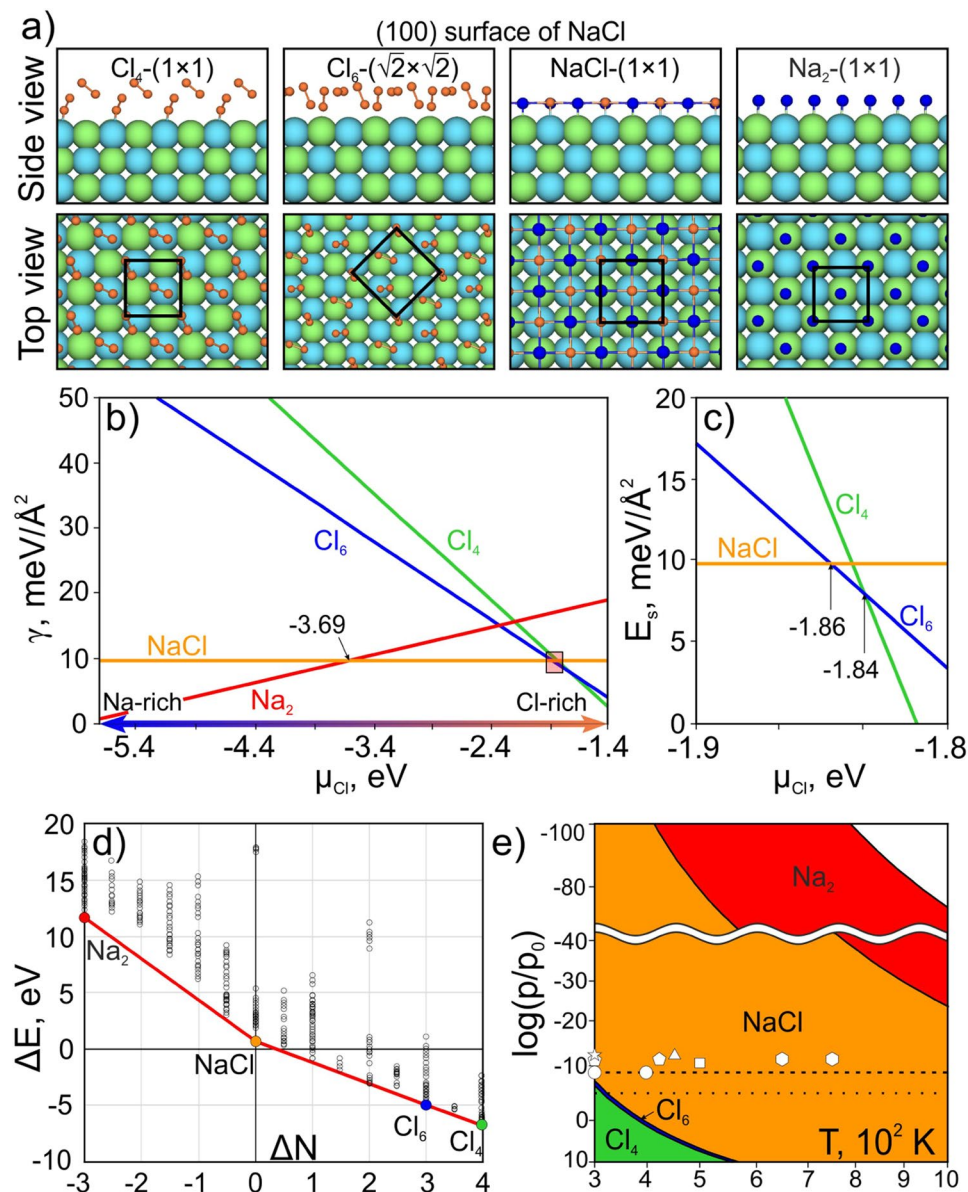


Figure 1. (a) The predicted reconstructions of the NaCl(100) surface. The chlorine atoms are shown in green, sodium atoms — in light blue. The surface atoms of chlorine and sodium are shown in orange and blue, respectively. (b) Surface energy as a function of μ_{Cl} . (c) The enlarged region for the μ_{Cl} range from -1.8 eV to -1.9 eV. (d) Convex hull diagram, where solid circles indicate thermodynamically stable reconstructions; the colors of the circles correspond to the colors of the lines in (b). (e) Phase diagram of the NaCl(100) surface. The experimental conditions of the heteroepitaxial growth of the (100) surface on various substrates are taken from refs^{10,11,19,20,22,52} and represented by various white shapes.

nonreconstructed (100) and (111) surfaces: $0.010 \text{ eV}/\text{\AA}^2$ and $0.030 \text{ eV}/\text{\AA}^2$, respectively, and these values are independent of the chemical potentials (the energies of reconstructed surfaces will, in general, depend on the chemical potentials, according to Eq. (6)). The polarity of the (111) surface leads to the formation of surprising surface phases like freestanding ultrathin NaCl films^{32,34}. Motivated by this, we tried to answer the following questions: How does the (111) surface change at nanoscale? Can we find any stable unexpected reconstructions?

To answer these questions, we performed a search and found five stable reconstructions of the NaCl(111) surface, namely, NaCl_6 -(1×1), NaCl-(1×1), Na_3Cl_2 -(1×1), Na_3Cl -(1×1), and Na_4 -(1×1), shown in Fig. 2a. As all these reconstructions have a 1×1 unit cell, we omit the “-(1×1)” part in their names below. There is one reconstruction with a high concentration of chlorine (NaCl_6 in panel (i) of Fig. 2a). Despite the additional Cl_2 molecules that chlorine forms on this surface, the NaCl_6 reconstruction has a corrugated “sawtooth-like” profile with sodium atoms (shown in dark blue) located at each vertex. Each facet of this surface reproduces the (100) surface of NaCl.

The nonreconstructed (111) NaCl surface is found to be slightly graphitized (panel (ii) in Fig. 2a). The top layer moves away from the substrate, forming a corrugated graphene-like structure. The graphitization process

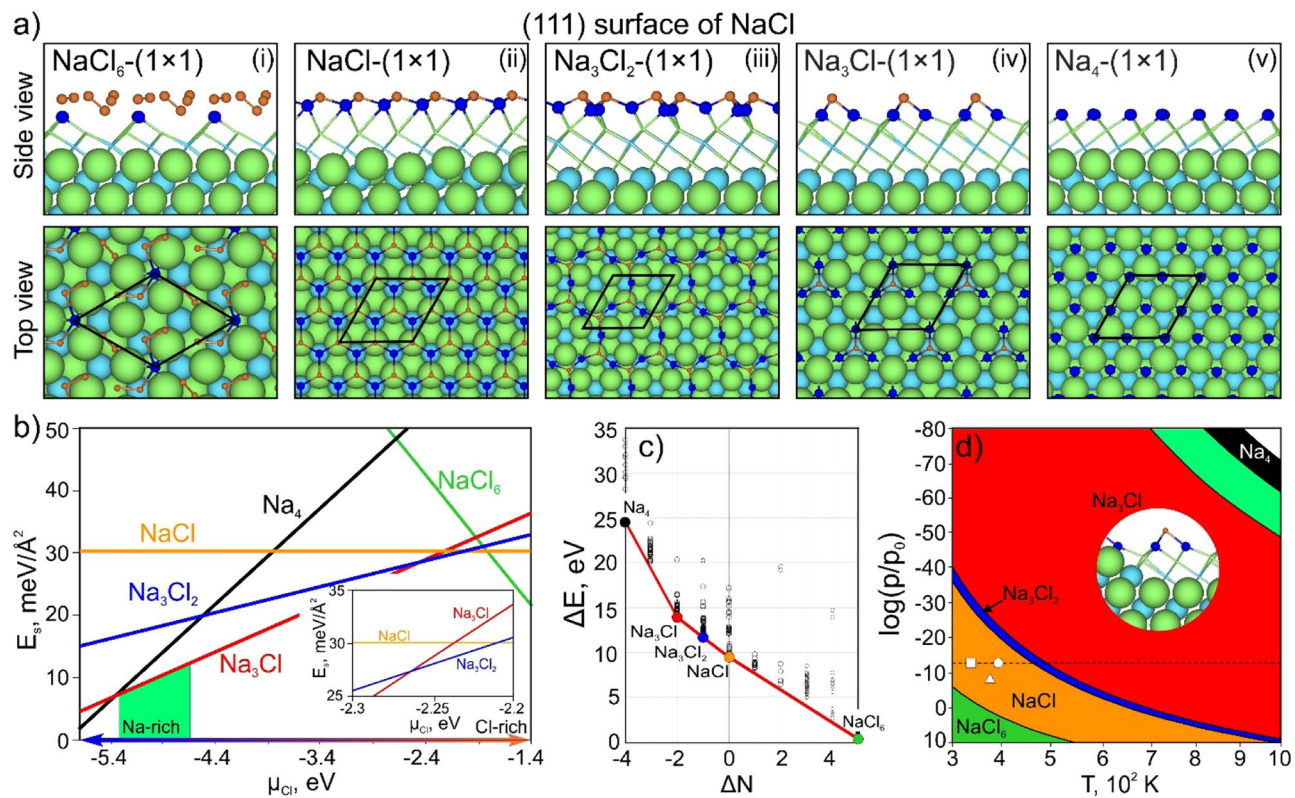


Figure 2. (a) Atomic structures of the predicted stable reconstructions of the (111) surface of NaCl: NaCl₆-(1 × 1), NaCl-(1 × 1), Na₃Cl₂-(1 × 1), Na₃Cl-(1 × 1), and Na₄-(1 × 1). (b) Surface energy as a function of μ_{Cl} . The region of $\mu_{Cl} = -2.2$ eV to -2.3 eV is shown enlarged in an inset. (c) Convex hull diagram, where solid circles indicate the thermodynamically stable surface phases; the colors of the circles correspond to the colors of the lines in (b). (d) Phase diagram of the (111) surface of NaCl. The dashed horizontal line corresponds to ultrahigh vacuum conditions (10^{-13} bar). Reference data on the experimental conditions of NaCl(111) growth on Si(100)-(2 × 1)³⁶, Si(111)-(7 × 7)³⁷, and GaAs(111)³⁵ substrates are represented by the small circle, square, and triangle, respectively. The light green region in (b) indicates the conditions at which Na₃Cl-(1 × 1) appears on the crystal shape according to the Wulff construction (in this case, it corresponds to $\gamma(111)/\gamma(100) < \sqrt{3}$).

like this helps to remove the surface dipole as was predicted earlier for freestanding ultrathin NaCl films with (111) surfaces³². However, here the substrate plays an important role leading to the corrugation of the outer layer in contrast to the freestanding films, though the distance between the layer and substrate is the same as for the thin graphitic NaCl films³² and equals 3.7 Å (panel (ii) of Fig. 2a). A very loose structure (top view in panel (iii) of Fig. 2a) of the Na₃Cl₂ reconstruction is stable in a very narrow range of chlorine chemical potentials, from -2.26 eV to -2.23 eV (inset in Fig. 2b). This reconstruction can be considered as transient between NaCl and Na₃Cl, where the regular structure of NaCl is lost.

In the Na₃Cl surface reconstruction (panel (iv) of Fig. 2a), the chlorine atoms in the outer layer form a sawtooth-like surface where each facet reproduces the (100) surface of NaCl. This surface is similar to NaCl₆ (if we disregard Cl₂) as both display the facets of (100). During the growth of the (111) surface of NaCl, a more stable surface (in this case (100)) will grow slower than (111) and a sawtooth-like surface with (100) facets will form. The Na₄ reconstruction represents the sodium-terminated (111) surface of NaCl (panel (v) in Fig. 2a).

Thermodynamic stability of the predicted reconstructions is shown in the computed surface energy diagram (Fig. 2b). The stability field of the chlorine-rich reconstruction NaCl₆ is relatively narrow, in the range of μ_{Cl} from -1.41 eV to -1.83 eV (green line in Fig. 2b). A chlorine-rich atmosphere is needed to obtain this reconstruction. Interestingly, the graphitic-like reconstruction of the (111) surface of NaCl is stable in the range of chlorine chemical potentials from -1.83 eV to -2.21 eV (orange line in Fig. 2b). The cleaved (111) surface of NaCl reconstructs to a graphene-like surface to compensate the surface dipole component normal to the (111) surface caused by the polarity of the surface (due to the alignment of atoms within one atomic plane). This is similar to the graphitization of thin freestanding NaCl films³². We found that the cleaved (111) nongraphitized surface is located very close to the convex hull line, being just 0.04 eV above it.

The Na₃Cl₂ reconstruction has a very narrow stability field at μ_{Cl} from -2.22 eV to -2.27 eV, which can also be seen from the convex hull diagram in Fig. 2c. The slope of the hull almost does not change, with the Na₃Cl₂ reconstruction point located almost exactly on the straight line between the Na₃Cl and NaCl reconstructions (Fig. 2c).

The widest stability field belongs to the Na₃Cl reconstruction. The convex hull has a strong cusp corresponding to this surface phase (Fig. 2c), which is stable in a wide range of chlorine chemical potentials, from -2.27 eV to -5.36 eV.

Next we define the range of values of the chlorine chemical potential at which the (111) surface will appear on the equilibrium shape of the crystal using the Wulff construction⁵⁵. In a single crystal of NaCl with predominant (100) surfaces, the (111) surface will exist only if $\gamma^{(111)}(\mu_{\text{Cl}})/\gamma^{(100)}(\mu_{\text{Cl}}) < \sqrt{3}$. Using the calculated surface energies as a function of chlorine chemical potential, for reconstructions of the (100) and (111) surfaces we found that at $\mu_{\text{Cl}} < -4.62$ eV the surface energy of $\text{Na}_3\text{Cl}-(1 \times 1)$ satisfies the above condition. However, at $\mu_{\text{Cl}} < -5.36$ eV the stable phase of the (100) surface changes: the $\text{Na}_2-(1 \times 1)$ reconstruction becomes stable (Fig. 1b). Taking this into account, we conclude that it is possible to obtain the $\text{Na}_3\text{Cl}-(1 \times 1)$ reconstruction of the (111) surface on the equilibrium shape of a NaCl crystal at -5.36 eV $< \mu_{\text{Cl}} < -4.62$ eV (Fig. 2b). The Wulff constructions for several values of μ_{Cl} are shown in Fig. S1 (see Supporting Information).

Let us consider the $P_{\text{Cl}_2} - T$ phase diagram for all the studied reconstructions (Fig. 2d). Here, the dashed line denotes the pressure of 10^{-13} bar, which corresponds to ultrahigh vacuum conditions. The conditions of the NaCl(111) surface formation on Si(100)-(2 × 1)³⁶ and Si(111)-(7 × 7)³⁷ substrates are within the calculated stability region of the heteroepitaxial growth of the (111) surface (marked by a small circle and square in Fig. 2d). The triangle in Fig. 2d indicates the chlorine pressure of 5×10^{-8} bar and the temperature of ~ 110 °C, corresponding to the experimental conditions from ref.³⁵. According to the calculated phase diagram, the formation of the Na_3Cl reconstruction should occur at high-temperature conditions (red region in Fig. 2d). We have translated the range of chlorine chemical potentials at which the (111) surface will appear into the temperature and partial pressure of chlorine (light green regions in Fig. 2d). The results show that the $\text{Na}_3\text{Cl}(111)$ reconstruction can be obtained as an equilibrium surface only at high temperatures > 700 K and extremely low chlorine pressures (Fig. 2d).

It is important that all the reconstructions of the (111) surface are polar (i.e. a different number of cations and anions is observed on the surface). According to the previous study of thin NaCl films³², to reduce the surface energy, the structure of thin films should minimize the dipole moment component normal to the surface. We studied the (111) surface reconstructions using Bader analysis (Figure 3), which gave the atomic charges in the bulk NaCl equal to $+0.83e$ and $-0.83e$ for the sodium and chlorine atoms, respectively. Fig. 3 shows the deviations of charges of the surface atoms from these values.

We found that the $\text{Na}_3\text{Cl}-(1 \times 1)$ reconstruction has no charge difference relative to the bulk values (Fig. 3b), while for the surface atoms of the $\text{NaCl}-(1 \times 1)$ and $\text{Na}_3\text{Cl}_2-(1 \times 1)$ reconstructions the charges are clearly different. The obtained charges of the surface Cl atoms were $-0.66e$ and $-0.69e$ on average (Fig. 3a,c) for the $\text{NaCl}-(1 \times 1)$ and $\text{Na}_3\text{Cl}_2-(1 \times 1)$ surface reconstructions, respectively, which is $0.17e$ and $0.13e$ lower in absolute values than that for the Cl atoms in the bulk NaCl, while Na atoms have the same charges as in the bulk. This reduces surface dipole. We should also mention, that these reconstructions are metallic.

Conclusions

Using the global optimization algorithm USPEX, we have studied a textbook case of the (100) and (111) surfaces of NaCl. The former is viewed as an archetypal “simple” surface: stable, stoichiometric, nonreconstructing, and nonpolar. The latter is regarded as a classical polar surface, normally unstable. Our results paint a much more complex picture. At extreme values of chemical potentials, we have found the deposition of Na (at low chemical potentials of Cl) and Cl (at high chemical potentials of Cl) and very low surface energies, which will lead to the embrittlement of NaCl in Na-rich and Cl-rich environments, a manifestation of the Rehbinder effect. On the (111) surface, we predict exotic stable surface compounds, $\text{NaCl}_6-(111)$ and $\text{Na}_3\text{Cl}-(111)$, which stabilize this polar surface, reducing its dipole moment. The new $\text{Na}_3\text{Cl}-(1 \times 1)$ reconstruction is found to have the widest range of stability among all the other compounds considered here for the (111) surface. Moreover, contrary to conventional thinking, we find from the Wulff theorem that the (111) surface with the $\text{Na}_3\text{Cl}-(1 \times 1)$ compound can be stable on the equilibrium shape in Na-rich conditions.

Computational details. Stable reconstructions of the NaCl surfaces were predicted using the first-principles evolutionary algorithm (EA) as implemented in the USPEX code^{38–40}, in its adaptation for surfaces⁴¹. In the presented calculations we included all the surface supercells up to index 4. Here, evolutionary searches were combined with structure relaxations using density functional theory (DFT)^{56,57} within the generalized gradient approximation (Perdew–Burke–Ernzerhof functional)⁵⁸ and projector-augmented wave method^{59,60} as implemented in the VASP^{61–63} package. The plane-wave energy cutoff of 500 eV and k -mesh of $2\pi \times 0.05\text{Å}^{-1}$ resolution ensure excellent convergence of the energy difference, stresses, and forces. Monopole, dipole, and quadrupole corrections were taken into account using the method discussed in refs.^{64,65}. During the structure search, the first generation was produced randomly, while subsequent generations were obtained by applying 40% heredity, 10% softmutation, and 20% transmutation operations, respectively, with 30% of each new generation produced using the random symmetric algorithm⁶⁶. Each of the studied supercells under study contained a vacuum layer with the thickness of 20 Å and a 6-Å-thick substrate slab of three NaCl layers for the (001) surface, with the topmost 3-Å layer allowed to relax, while for the (111) surface a substrate slab of ~ 8 Å was chosen, with the topmost 3-Å layer allowed to relax.

To perform variable-composition searches for stable surface reconstructions, it is important to set the boundary values of the physically allowed chemical potentials, which are related to the free energies of bulk Na, Cl₂ gas, and bulk NaCl. The surface energies of the predicted reconstructions were calculated as

$$\gamma = \frac{1}{N} \left[E_{\text{tot}} - E_{\text{ref}} - \sum_i n_i \mu_i \right] \quad (3)$$

where E_{tot} is the total energy of the whole system, E_{ref} is the reference energy of the substrate (the unreconstructed cleaved (100) or (111) surface), n_i is the number of additional atoms of type i (Na or Cl) on the substrate, μ_i is

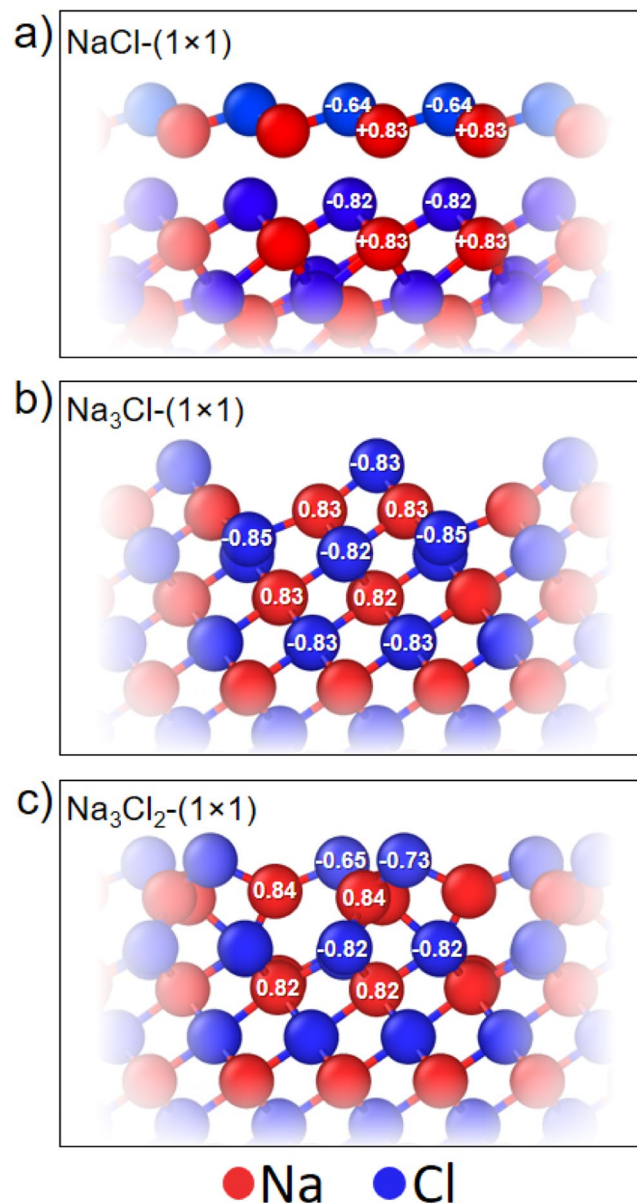


Figure 3. Bader charges (to be compared with the bulk values of +0.83 for Na and −0.83 for Cl) for the (111) surface reconstructions of NaCl including (a) NaCl-(1 × 1), (b) Na₃Cl-(1 × 1), and (c) Na₃Cl₂-(1 × 1). The red and blue colors depicted sodium and chlorine atoms.

the chemical potential of the atom of type i , $N = m \times n$ for an $m \times n$ surface supercell (serves as a normalization factor).

In the case of NaCl, Eq. (3) becomes

$$\gamma(T, P) = \frac{1}{N} [G^{slab}(T, P, N_{Na}, N_{Cl}) - N_{Na} \mu_{Na}(T, P) - N_{Cl} \mu_{Cl}(T, P)], \quad (4)$$

where $\gamma(T, P)$ is the surface energy per surface area, $G^{slab}(T, P, N_{Na}, N_{Cl})$ is the Gibbs free energy of the surface per cell, N_{Na} , μ_{Na} and N_{Cl} , μ_{Cl} are the number and chemical potential of the Na and Cl atoms in the cell, respectively.

The chemical potentials in equilibrium with the NaCl substrate are related in the following way:

$$\mu_{Na}(T, P) + \mu_{Cl}(T, P) = G_{NaCl}(T, P), \quad (5)$$

where $G_{NaCl}(T, P)$ is the Gibbs free energy of the bulk NaCl. Thus, surface energy can be expressed in a form with only one variable chemical potential:

$$\gamma(T, P) = \frac{1}{N} [G^{slab}(T, P, N_{Na}, N_{Cl}) - N_{Na} G_{NaCl}^{bulk}(T, P) - (N_{Cl} - N_{Na}) \mu_{Cl}(T, P)] \quad (6)$$

The lower limit of the chemical potential was set as the chemical potential of Cl at which Na deposits on the substrate, while the upper limit corresponds to the case where Cl₂ molecules are saturated on the substrate. The following relation defines the physically meaningful range of chemical potentials:

$$\frac{1}{2}\Delta E_f(T, P) + \frac{1}{2}E_{Cl_2} \leq \mu_{Cl}(T, P) \leq \frac{1}{2}E_{Cl_2}, \quad (7)$$

where E_{Cl_2} is the total energy of a chlorine molecule, $\Delta E_f(T, P) = 4.17$ eV is the energy of formation of the bulk rock-salt NaCl, which is in close agreement with the experimental value of 3.98 eV at room temperature^{67,68}.

Stability of different structures can be compared using Eq. (6) by plotting γ as a function of μ_{Cb} as shown in Figs 1b and 2b. Each structure corresponds to a line on the phase diagram. A complementary and equivalent way to determine stability is to plot the convex hull diagram (Figs 1c and 2c) in ΔE - ΔN axes⁴¹, where

$$\Delta E = \frac{1}{N}[G^{slab}(T, P, N_{Na}, N_{Cl}) - N_{Na}G_{NaCl}^{bulk}(T, P)] \text{ and } \Delta N = \frac{1}{N}(N_{Na} - N_{Cl}) \quad (8)$$

References

- Bassett, W. A., Takahashi, T., Mao, H. & Weaver, J. S. Pressure-Induced Phase Transformation in NaCl. *J Appl Phys* **39**(1), 319–325 (1968).
- Froyen, S. & Cohen, M. L. Structural properties of NaCl. *Phys Rev B* **29**(6), 3770–3772 (1984).
- Li, X. & Jeanloz, R. Measurement of the B1-B2 transition pressure in NaCl at high temperatures. *Phys Rev B* **36**(1), 474–479 (1987).
- Čančarević, Ž. P., Christian, S. J. & Jansen, M. Stability of Alkali Metal Halide Polymorphs as a Function of Pressure. *Chem Asian J.* **3**(3), 561–572 (2008).
- Zhang, W. *et al.* Unexpected stable stoichiometries of sodium chlorides. *Science* **342**(6165), 1502–1505, <https://doi.org/10.1126/science.1244989> (2013).
- Shi, G. *et al.* Two-dimensional Na–Cl crystals of unconventional stoichiometries on graphene surface from dilute solution at ambient conditions. *Nat. Chem.* **10**(7), 776 (2018).
- Tasker, P. W. The surface energies, surface tensions and surface structure of the alkali halide crystals. *Phil Mag A* **39**(2), 119–136, <https://doi.org/10.1080/01418617908236887> (1979).
- MacDonald, R. J., Taglauer, E. C. & Wandelt, K. *Surface Science - Principles and Current Applications*. Surface Science - Principles and Current Applications, 1st ed.; Springer Berlin Heidelberg, 1996.
- Surface Science: Foundations of Catalysis and Nanoscience. *Surface Science: Foundations of Catalysis and Nanoscience*, 3rd ed.; Kolasinski, K. W., Ed.; Wiley, 2002.
- Guo, Q. *et al.* Bias dependence of apparent layer thickness and Moiré pattern on NaCl/Cu(001). *Surf. Sci.* **604**(19), 1820–1824 (2010).
- Kiguchi, M., Entani, S., Saiki, K., Inoue, H. & Koma, A. Two types of epitaxial orientations for the growth of alkali halide on fcc metal substrates. *Phys. Rev. B* **66**(15), 155424 (2002).
- Wagner, M. *et al.* Nanostripe Pattern of NaCl Layers on Cu(110). *Phys. Rev. Lett.* **110**(21), 216101 (2013).
- Bennewitz, R. *et al.* Aspects of dynamic force microscopy on NaCl/Cu(111): resolution, tip-sample interactions and cantilever oscillation characteristics. *Surf. Interface Anal.* **27**(5–6), 462–466 (1999).
- Bennewitz, R. *et al.* Atomically resolved edges and kinks of NaCl islands on Cu(111): Experiment and theory. *Phys. Rev. B* **62**(3), 2074–2084 (2000).
- Repp, J., Meyer, G., Paavilainen, S., Olsson, F. E. & Persson, M. Scanning Tunneling Spectroscopy of Cl Vacancies in NaCl Films: Strong Electron-Phonon Coupling in Double-Barrier Tunneling Junctions. *Phys. Rev. Lett.* **95**(22), 225503 (2005).
- Mishima, R., Takada, M. & Tada, H. STM Studies of NaCl Thin Films on Cu(111) Surface at Low Temperature. *Mol. Cryst. Liq. Cryst.* **472**(1), 321/[711]–325/[715] (2007).
- Li, Y. J. *et al.* Force Mapping of the NaCl(100)/Cu(111) Surface by Atomic Force Microscopy at 78 K. *Jpn. J. Appl. Phys.* **51**(3R), 035201 (2012).
- Kakudate, T., Nakaya, M. & Nakayama, T. Local modification of NaCl thin films on Cu(111) under different bias voltages. *Thin Solid Films* **520**(6), 2004–2008 (2012).
- Gerß, B., Osterloh, N., Heidorn, S.-C. & Morgenstern, K. Diffusion Limited Aggregation in Low Temperature Growth of Sodium Chloride. *Cryst. Growth Des.* **15**(6), 3046–3051 (2015).
- Riemann, A., Fölsch, S. & Rieder, K. H. Epitaxial growth of alkali halides on stepped metal surfaces. *Phys. Rev. B* **72**(12), 125423 (2005).
- Fölsch, S. *et al.* Self-Organized Patterning of an Insulator-on-Metal System by Surface Faceting and Selective Growth: NaCl/Cu(211). *Phys. Rev. Lett.* **84**(1), 123–126 (2000).
- Pivetta, M., Patthey, F., Stengel, M., Baldereschi, A. & Schneider, W.-D. Local work function Moiré pattern on ultrathin ionic films: NaCl on Ag(100). *Phys. Rev. B* **72**(11), 115404 (2005).
- Matthaei, F. *et al.* Coulomb attraction during the carpet growth mode of NaCl. *J Phys Condens Matter* **24**(35), 354006 (2012).
- Cabailh, G., Henry, C. R. & Barth, C. Thin NaCl films on silver (001): island growth and work function. *New J. Phys.* **14**(10), 103037 (2012).
- Heidorn, S. *et al.* Influence of Substrate Surface-Induced Defects on the Interface State between NaCl(100) and Ag(111). *J. Phys. Chem. C* **117**(31), 16095–16103 (2013).
- Heidorn, S.-C., Sabellek, A. & Morgenstern, K. Size Dependence of the Dispersion Relation for the Interface State between NaCl(100) and Ag(111). *Nano Lett* **14**(1), 13–17 (2013).
- Sun, X., Felicissimo, M. P., Rudolf, P. & Silly, F. NaCl multi-layer islands grown on Au(111)-(22)times \sqrt{3} probed by scanning tunneling microscopy. *Nanotechnology* **19**(49), 495307 (2008).
- Clayssens, F. *et al.* Growth of ZnO thin films—experiment and theory. *J Mater Chem* **15**, 139–148 (2005).
- Lee, J., Sorescu, D. C. & Deng, X. Tunable Lattice Constant and Band Gap of Single- and Few-Layer ZnO. *J. Phys. Chem. Lett.* **7**(7), 1335–1340 (2016).
- Lin, S. S. Light-Emitting Two-Dimensional Ultrathin Silicon Carbide. *J Phys Chem C* **116**(6), 3951–3955 (2012).
- Tsipas, P. *et al.* Evidence for graphite-like hexagonal AlN nanosheets epitaxially grown on single crystal Ag(111). *Appl. Phys. Lett.* **103**(25), 251605–251608 (2013).
- Kvashnin, A. G., Sorokin, P. B. & Tománek, D. Graphitic Phase of NaCl. Bulk Properties and Nanoscale Stability. *J. Phys. Chem. Lett.* **5**(22), 4014–4019 (2014).
- Sorokin, P. B., Kvashnin, A. G., Zhu, Z. & Tománek, D. Spontaneous Graphitization of Ultrathin Cubic Structures: A Computational Study. *Nano Lett.* **14**(12), 7126–7130 (2014).
- Kvashnin, A. G.; Pashkin, E. Y.; Yakobson, B. I. & Sorokin, P. B. Ionic Graphitization of Ultrathin Films of Ionic Compounds. *J. Phys. Chem. Lett.* 2659–2663 (2016).

35. Saiki, K., Goda, A. & Koma, A. Growth of Polar NaCl(111) Surface on GaAs(111) Substrates. *Jpn. J. Appl. Phys.* **36**(1A), L55 (1997).
36. Chung, J.-Y., Li, H.-D., Chang, W.-H., Leung, T. C. & Lin, D.-S. Sodium chloride on Si(100) grown by molecular beam epitaxy. *Phys. Rev. B* **83**(8), 085305 (2011).
37. Beinik, I., Barth, C., Hanbücken, M. & Masson, L. KCl ultra-thin films with polar and non-polar surfaces grown on Si(111)7 × 7. *Sci. Rep.* **5**, (2015).
38. Oganov, A. R. & Glass, C. W. Crystal structure prediction using ab initio evolutionary techniques: Principles and applications. *J. Chem Phys* **124**, 244704 (2006).
39. Oganov, A. R., Lyakhov, A. O. & Valle, M. How Evolutionary Crystal Structure Prediction Works—and Why. *Acc. Chem. Res.* **44**, 227–237 (2011).
40. Lyakhov, A. O., Oganov, A. R., Stokes, H. T. & Zhu, Q. New developments in evolutionary structure prediction algorithm USPEX. *Comput. Phys. Commun.* **184**, 1172–1182 (2013).
41. Zhu, Q., Li, L., Oganov, A. R. & Allen, P. B. Evolutionary method for predicting surface reconstructions with variable stoichiometry. *Phys. Rev. B* **87**, 19 (2013).
42. Wang, Q., Oganov, A. R., Zhu, Q. & Zhou, X.-F. New Reconstructions of the (110) Surface of Rutile TiO_2 Predicted by an Evolutionary Method. *Phys. Rev. Lett.* **113**(26), 266101 (2014).
43. Zakaryan, H. A., Kvashnin, A. G. & Oganov, A. R. Stable reconstruction of the (110) surface and its role in pseudocapacitance of rutile-like RuO_2 . *Sci. Rep.* **7**(1), 10357 (2017).
44. Barth, C. & Henry, C. R. Surface Double Layer on (001) Surfaces of Alkali Halide Crystals: A Scanning Force Microscopy Study. *Phys. Rev. Lett.* **98**(13), 136804 (2007).
45. Bombis, C. *et al.* Hydrogen-Bonded Molecular Networks of Melamine and Cyanuric Acid on Thin Films of NaCl on Au111. *Small* **5**(19), 2177–2182 (2009).
46. Griffith, A. A. The Phenomena of Rupture and Flow in Solids. *Philos. Trans. R. Soc. Lond. Math. Phys. Eng. Sci.* **221**(582–593), 163–198 (1921).
47. Rehbinder, P. A. & Logginov, G. I. Changes in the elastic properties of mica during the metal penetration of a liquid in deformed metal. *Dokl Akad Nauk SSSR* **30**(6), 489–494 (1941).
48. Andrade, E. N. D. A. C., Randall, R. F. Y. & Makin, M. J. The Rehbinder Effect. *Proc. Phys. Soc. Sect. B* **63**(12), 990–995 (1950).
49. Rehbinder, P. A. & Shchukin, E. D. Surface phenomena in solids during the course of their deformation and failure. *Sov. Phys. Uspekhi* **15**(5), 533 (1973).
50. Andrade, E. N. D. C. & Randall, R. F. Y. The Rehbinder Effect. *Nature* **164**(4183), 1127 (1949).
51. NIST, Chemistry WebBook. NIST, Chemistry WebBook, <http://webbook.nist.gov/>.
52. Chen, P., Kuttipillai, P. S., Wang, L. & Lunt, R. R. Homoepitaxial Growth of Metal Halide Crystals Investigated by Reflection High-Energy Electron Diffraction. *Sci. Rep.* **7** (2017).
53. Bruno, M., Aquilano, D., Pastero, L. & Prencepe, M. Structures and Surface Energies of (100) and Octopolar (111) Faces of Halite (NaCl): an Ab initio Quantum-Mechanical and Thermodynamical Study. *Cryst Growth Des* **8**(7), 2163–2170 (2008).
54. Wolf, D. Reconstruction of NaCl surfaces from a dipolar solution to the Madelung problem. *Phys. Rev. Lett.* **68**(22), 3315–3318 (1992).
55. Wulff, G. Z. F. *der Geschwindigkeit des Wachstums und der Auflösung der Kristallflächen.* *Z. Für Krist. - Cryst. Mater.* **34**(1–6), 449–530 (1901).
56. Hohenberg, P. & Kohn, W. Inhomogeneous electron gas. *Phys Rev* **136**(3B), B864–B871 (1964).
57. Kohn, W. & Sham, L. J. Self-consistent equations including exchange and correlation effects. *Phys Rev* **140**(4), A1133–A1138 (1965).
58. Perdew, J. P., Burke, K. & Ernzerhof, M. Generalized gradient approximation made simple. *Phys. Rev. Lett.* **77**(18), 3865–3868 (1996).
59. Blöchl, P. E. Projector augmented-wave method. *Phys. Rev. B* **50**(24), 17953–17979 (1994).
60. Kresse, G. & Joubert, D. From ultrasoft pseudopotentials to the projector augmented-wave method. *Phys. Rev. B* **59**(3), 1758–1775 (1999).
61. Kresse, G. & Hafner, J. Ab initio molecular dynamics for liquid metals. *Phys. Rev. B* **47**(1), 558–561 (1993).
62. Kresse, G. & Hafner, J. Ab initio molecular-dynamics simulation of the liquid-metal-amorphous-semiconductor transition in germanium. *Phys. Rev. B* **49**(20), 14251–14269 (1994).
63. Kresse, G. & Furthmüller, J. Efficient iterative schemes for ab initio total-energy calculations using a plane-wave basis set. *Phys. Rev. B* **54**(16), 11169–11186 (1996).
64. Makov, G. & Payne, M. C. Periodic boundary conditions in ab initio calculations. *Phys. Rev. B* **51**(7), 4014–4022 (1995).
65. Neugebauer, J. & Scheffler, M. Adsorbate-substrate and adsorbate-adsorbate interactions of Na and K adlayers on Al(111). *Phys. Rev. B* **46**(24), 16067–16080 (1992).
66. Zhu, Q., Oganov, A. R., Glass, C. W. & Stokes, H. T. Constrained evolutionary algorithm for structure prediction of molecular crystals: methodology and applications. *Acta Crystallogr. B* **68**(3), 215–226 (2012).
67. Chase, N. W. *et al.* JANAF Thermochemical Tables. JANAF Thermochemical Tables, 3rd ed. In *J. Phys. Chem. Ref. Data.*; Suppl. 1; Vol. 14 (1985).
68. Chu, D.-Y., Zhang, Q. & Liu, R.-L. Standard Gibbs free energies of transfer of NaCl and KCl from water to mixtures of the four isomers of butyl alcohol with water. The use of ion-selective electrodes to study the thermodynamics of solutions. *J. Chem. Soc. Faraday Trans. 1 Phys. Chem. Condens. Phases* **83**(3), 635–644 (1987).

Acknowledgements

The work was supported by the Russian Science Foundation (№ 18-73-10135). The calculations were performed on Rurik supercomputer at the MIPT and on Arkuda supercomputer of the Skolkovo Foundation. We also thank the CSC-IT Center for Science Ltd, Finland, for generous grants of computer time.

Author Contributions

A.G.K., D.G.K. and A.R.O. directed work and designed the project. A.G.K. and D.G.K. performed the simulations. A.G.K., D.G.K. and A.R.O. analyzed the results and finalized the paper.

Additional Information

Supplementary information accompanies this paper at <https://doi.org/10.1038/s41598-019-50548-8>.

Competing Interests: The authors declare no competing interests.

Publisher's note Springer Nature remains neutral with regard to jurisdictional claims in published maps and institutional affiliations.



Open Access This article is licensed under a Creative Commons Attribution 4.0 International License, which permits use, sharing, adaptation, distribution and reproduction in any medium or format, as long as you give appropriate credit to the original author(s) and the source, provide a link to the Creative Commons license, and indicate if changes were made. The images or other third party material in this article are included in the article's Creative Commons license, unless indicated otherwise in a credit line to the material. If material is not included in the article's Creative Commons license and your intended use is not permitted by statutory regulation or exceeds the permitted use, you will need to obtain permission directly from the copyright holder. To view a copy of this license, visit <http://creativecommons.org/licenses/by/4.0/>.

© The Author(s) 2019